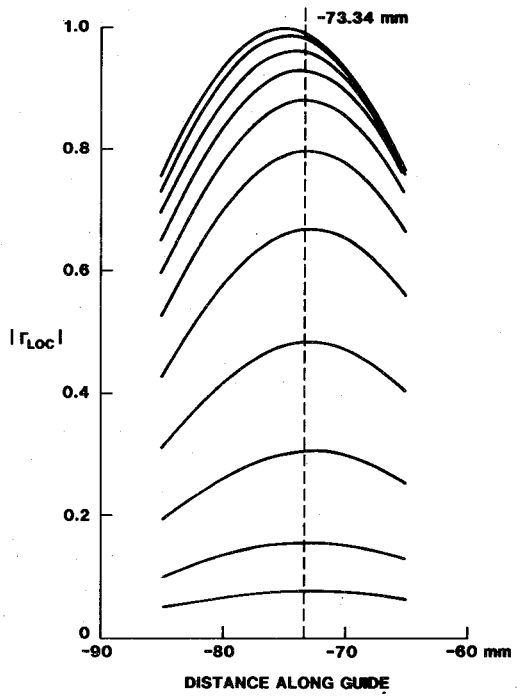

Fig. 3. Expanded view of the peaks of the magnitudes of the locating vectors for the balls measured versus distance. The shift of the peaks toward the source for large balls is easily seen.

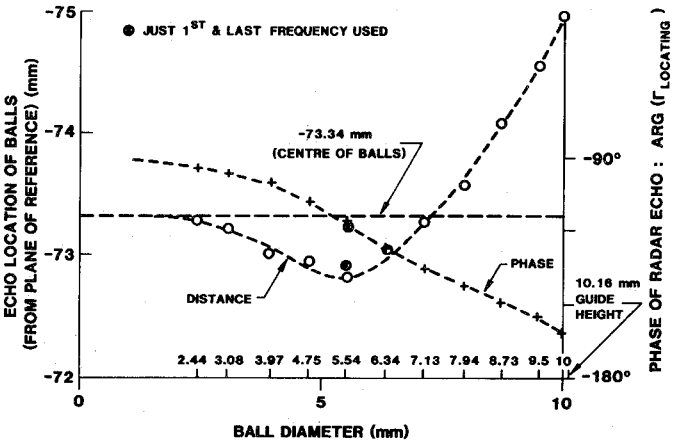

Fig. 4. Computed positions of the peak of the radar-echo, and arg(Γ(time)) versus ball diameter. It is seen that small balls appear to be farther away than their centers. Echoes of large balls move closer to the source. As a cross-check, the points indicated by × were computed using the first and last frequencies only.

susceptance in the center. Since the guide wavelength in the tapered section lengthens, the shunt susceptance appears to be farther away (group-delay is increased). For very large balls, this taper is very severe (guides tending toward cutoff), and dominates over the effect of the shunt susceptance and thus puts the reflection forward.

The experimental uncertainty in the echo locations is difficult to state, but repeated measurements produced very similar results. The individual departures of the points on Fig. 4 from the smooth fitted curve give an indication of the scatter. As a cross-check, the point corresponding to the largest, seemingly anomalous, echo location was computed using only the two extreme frequencies of the set of eleven, and reproduced the

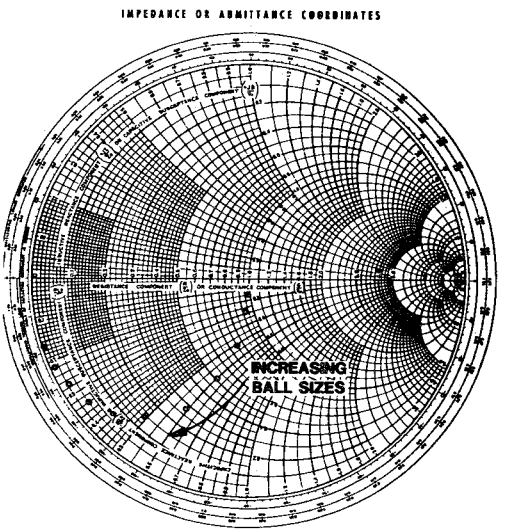

Fig. 5. The locating vector evaluated at its maximum, plotted on the Smith-chart for varying ball sizes. A resemblance to a capacitive obstacle is recognizable. Note that the locating vector is in the time domain.

trend of the results of the full set, as shown in Fig. 4.

In Fig. 4, the computed phase of the locating vector is shown at the echo-maxima. For small balls, the phase tends toward −90°, meaning that small balls may be regarded as lumped capacitive obstacles, whereas large balls exhibit phases which approach 180°, the expected value for an impedance which approaches a short circuit.

The Smith-chart plot of the complex locating vector (Fig. 5) indicates a quasi-capacitive behavior for all ball sizes. The departure from purely capacitive loading is attributed to the breakdown of the lumped element approximation as the balls become larger and the impedance is distributed along the waveguide.

References

[1] P. I. Somlo, "Conductive contacting spheres on the centre of the broad wall of rectangular waveguides," *Electron. Lett.*, vol. 8, no. 20, 1972.
[2] J. H. Hinken, "Conducting spheres in rectangular waveguides," *IEEE Trans. Microwave Theory Tech.*, vol. MTT-28, July 1980.
[3] P. I. Somlo, "The locating reflectometer," *IEEE Trans. Microwave Theory Tech.*, vol. MTT-20, Feb. 1972.
[4] J. Appel-Hansen, "Near-field cross sections and reflection centres for large spheres and plates—A fundamental analysis," *Tech. Univ. of Denmark*, Report R231, 1980. Also in *Antenna and Scattering Seminar*, (NML Australia) 1982.
[5] P. I. Somlo and J. D. Hunter, "A six-port reflectometer and its complete characterization by convenient calibration procedures," *IEEE Trans. Microwave Theory Tech.*, vol. MTT-30, Feb. 1982.
[6] P. I. Somlo, "Time-domain reflectometry from Smith-chart plotting," *Electron. Lett.*, vol. 9, no. 10, 1973.

Propagation on a Sheath Helix in a Coaxially Layered Lossy Dielectric Medium

MARK J. HAGMANN, MEMBER, IEEE

***Abstract*—Radial and axial dependence of the azimuthally symmetric fields in each coaxial layer may be expressed in terms of modified Bessel**

Manuscript received April 26, 1982; revised August 3, 1983.
The author is with the Biomedical Engineering and Instrumentation Branch, Division of Research Services, National Institutes of Health, Bethesda, MD 20205

functions and complex exponentials, respectively. There are two unknown coefficients in expressions for the innermost and outermost layers, and four in each of the other layers. Equations derived from boundary conditions are cascaded so that coefficients in the two layers adjacent to the helix are obtained as linear functions of coefficients in the innermost and outermost layers. Application of boundary conditions at the sheath helix results in an error term allowing an iterative solution for the complex axial propagation constant. An example of an inhomogeneous bone/muscle/fat/skin model of the human upper arm is used to test suitability of the helical coil in hyperthermia for the treatment of cancer. Deep, relatively uniform, deposition of energy may be obtained.

I. Introduction

The helical coil, in addition to its use in the traveling-wave tube (TWT) [1], has been considered for many other applications, including drying continuous filaments by microwave heating [2] and hyperthermia for the treatment of cancer [3]. It is necessary to modify the original treatment by Sensiper [4] to include regions having different dielectric properties in order to improve the realism of modeling in some of these applications. In particular, skin–fat–muscle dielectric layering has been shown to alter the coupling of electromagnetic energy to the human body [5], so such layering must be considered when modeling systems for use in hyperthermia.

Several methods have been used to correct for the presence of different dielectrics. An approximation valid at high frequencies has been used to simplify the analytical solution for a sheath helix having either coaxial dielectric layers [6] or wedge-shaped dielectric supports that are spaced periodically in the angular coordinate about the helix axis [7]. Equivalent circuit parameters have also been used to obtain the approximate dispersion characteristics of a helix perturbed by the presence of various dielectric and metallic objects [8], [9]. In evaluation of the helical coil as an applicator for use in hyperthermia, solutions are required for the local field values over a wide range of frequencies. None of the methods just described are considered suitable. A new method having high numerical efficiency is presented in this paper.

No rigorous solution has yet been found for a helix having realistic round wire. All work presented in this paper is for the sheath helix model [1], [4] in which the helix is replaced with a cylindrical shell having anisotropic conductivity that is infinite and zero in directions, respectively, parallel and normal to the original winding. Since all models have coaxial layering, only azimuthally symmetric modes are considered.

II. Analysis

It may be verified by direct substitution that the following expressions correspond to a general solution of Maxwell's equations within the ith layer of a system of N coaxial dielectric layers:

$$E_{zi} = [A_i I_0(\tau_i r) + C_i K_0(\tau_i r)]\, e^{j(\omega t - \beta z)} \tag{1}$$

$$E_{\theta i} = \frac{-j\omega\mu_i}{\tau_i}[B_i I_1(\tau_i r) - D_i K_1(\tau_i r)]\, e^{j(\omega t - \beta z)} \tag{2}$$

$$E_{ri} = \frac{j\beta}{\tau_i}[A_i I_1(\tau_i r) - C_i K_1(\tau_i r)]\, e^{j(\omega t - \beta z)} \tag{3}$$

$$H_{zi} = [B_i I_0(\tau_i r) + D_i k_0(\tau_i r)]\, e^{j(\omega t - \beta z)} \tag{4}$$

$$H_{\theta i} = \frac{j\omega\epsilon_i}{\tau_i}[A_i I_1(\tau_i r) - C_i K_1(\tau_i r)]\, e^{j(\omega t - \beta z)} \tag{5}$$

$$H_{ri} = \frac{j\beta}{\tau_i}[B_i I_1(\tau_i r) - D_i K_1(\tau_i r)]\, e^{j(\omega t - \beta z)} \tag{6}$$

where r is the radial distance from the axis of the helix, z is the longitudinal coordinate parallel to the axis, ω is the angular frequency of excitation, μ_i, ϵ_i are the permeability and permittivity of the ith layer, $j = \sqrt{-1}$, and I_γ, K_γ are the modified Bessel functions of the first and second kind, respectively.

Consistency with Maxwell's equations also requires that

$$\tau_i^2 = \beta^2 - k_i^2 \tag{7}$$

where $k_i = \omega\sqrt{\mu_i\epsilon_i}$, and β has the same value in each layer.

Since $K_\gamma(0)$ and $I_\gamma(\infty)$ diverge [10], we require that the coefficients C_1, D_1 in the innermost layer (containing the axis) and A_N, B_N in the outermost (infinite) layer must be identically zero.

The number of unknown coefficients is $4(N-1)$. Since β is also unknown, the total number of unknowns is $4N-3$. Boundary conditions provide four independent equations at each boundary. There is one additional equation relating the sheet current density (normalized to unity) to the magnetic field intensity in the two dielectric layers adjacent to the helix. Thus the total number of independent equations is $4N-3$, and the system is determined.

Others have used the high-frequency approximation $\beta \approx \tau$ [6], [7] to allow solving the system of simultaneous equations. If this or other approximations are not used, then the dependence of the matrix elements on the unknown parameter β would appear to require that iterations be used in which a new matrix is generated and inverted once each cycle. This would be impractical if many coaxial layers were required. The procedure to be described has high numerical efficiency since no matrix inversions are required. No approximations other than the sheath helix model have been required in this procedure.

For a boundary not on the sheath helix, it is required that E_z, E_θ, D_r, and H_z be continuous. Let r_i be defined as the outer radius of the ith coaxial layer. Then, using a Wronskian for simplification, the four equations from boundary conditions may be manipulated to give the following system for upward recursion in the unknown coefficients:

$$A_{i+1} = \tau_{i+1} r_i \left[A_i \left[I_0(\tau_i r_i) K_1(\tau_{i+1} r_i) + \frac{\epsilon_i \tau_{i+1}}{\epsilon_{i+1} \tau_i} I_1(\tau_i r_i) K_0(\tau_{i+1} r_i) \right] + C_i \left[K_0(\tau_i r_i) K_1(\tau_{i+1} r_i) - \frac{\epsilon_i \tau_{i+1}}{\epsilon_{i+1} \tau_i} K_1(\tau_i r_i) K_0(\tau_{i+1} r_i) \right] \right] \tag{8}$$

$$C_{i+1} = \tau_{i+1} r_i \left[A_i \left[I_0(\tau_i r_i) I_1(\tau_{i+1} r_i) - \frac{\epsilon_i \tau_{i+1}}{\epsilon_{i+1} \tau_i} I_1(\tau_i r_i) I_0(\tau_{i+1} r_i) \right] + C_i \left[K_0(\tau_i r_i) I_1(\tau_{i+1} r_i) + \frac{\epsilon_i \tau_{i+1}}{\epsilon_{i+1} \tau_i} K_1(\tau_i r_i) I_0(\tau_{i+1} r_i) \right] \right] \tag{9}$$

$$B_{i+1} = \tau_{i+1} r_i \left[B_i \left[I_0(\tau_i r_i) K_1(\tau_{i+1} r_i) + \frac{\mu_i \tau_{i+1}}{\mu_{i+1} \tau_i} I_1(\tau_i r_i) K_0(\tau_{i+1} r_i) \right] + D_i \left[K_0(\tau_i r_i) K_1(\tau_{i+1} r_i) - \frac{\mu_i \tau_{i+1}}{\mu_{i+1} \tau_i} K_1(\tau_i r_i) K_0(\tau_{i+1} r_i) \right] \right] \tag{10}$$

$$D_{i+1} = \tau_{i+1} r_i \left[\begin{array}{l} B_i \left[I_0(\tau_i r_i) I_1(\tau_{i+1} r_i) - \frac{\mu_i \tau_{i+1}}{\mu_{i+1} \tau_i} I_1(\tau_i r_i) I_0(\tau_{i+1} r_i) \right] \\ + D_i \left[K_0(\tau_i r_i) I_1(\tau_{i+1} r_i) + \frac{\mu_i \tau_{i+1}}{\mu_{i+1} \tau_i} K_1(\tau_i r_i) I_0(\tau_{i+1} r_i) \right] \end{array} \right]. \quad (11)$$

Alternatively, the following equations may be obtained for downward recursion in the coefficients where, again, r_i must not be the boundary at the sheath helix:

$$A_i = \tau_i r_i \left[\begin{array}{l} A_{i+1} \left[I_0(\tau_{i+1} r_i) K_1(\tau_i r_i) + \frac{\epsilon_{i+1} \tau_i}{\epsilon_i \tau_{i+1}} I_1(\tau_{i+1} r_i) K_0(\tau_i k_i) \right] \\ + C_{i+1} \left[K_0(\tau_{i+1} r_i) K_1(\tau_i r_i) - \frac{\epsilon_{i+1} \tau_i}{\epsilon_i \tau_{i+1}} K_1(\tau_{i+1} r_i) K_0(\tau_i r_i) \right] \end{array} \right] \quad (12)$$

$$C_i = \tau_i r_i \left[\begin{array}{l} A_{i+1} \left[I_0(\tau_{i+1} r_i) I_1(\tau_i r_i) - \frac{\epsilon_{i+1} \tau_i}{\epsilon_i \tau_{i+1}} I_1(\tau_{i+1} r_i) I_0(\tau_i - r_i) \right] \\ + C_{i+1} \left[K_0(\tau_{i+1} r_i) I_1(\tau_i r_i) + \frac{\epsilon_{i+1} \tau_i}{\epsilon_i \tau_{i+1}} K_1(\tau_{i+1} r_i) I_0(\tau_i r_i) \right] \end{array} \right] \quad (13)$$

$$B_i = \tau_i r_i \left[\begin{array}{l} B_{i+1} \left[I_0(\tau_{i+1} r_i) K_1(\tau_i r_i) + \frac{\mu_{i+1} \tau_i}{\mu_i \tau_{i+1}} I_1(\tau_{i+1} r_i) K_0(\tau_i r_i) \right] \\ + D_{i+1} \left[K_0(\tau_{i+1} r_i) K_1(\tau_i r_i) - \frac{\mu_{i+1} \tau_i}{\mu_i \tau_{i+1}} K_1(\tau_{i+1} r_i) K_0(\tau_i r_i) \right] \end{array} \right] \quad (14)$$

$$D_i = \tau_i r_i \left[\begin{array}{l} B_{i+1} \left[I_0(\tau_{i+1} r_i) I_1(\tau_i r_i) - \frac{\mu_{i+1} \tau_i}{\mu_i \tau_{i+1}} I_1(\tau_{i+1} r_i) I_0(\tau_i r_i) \right] \\ + D_{i+1} \left[K_0(\tau_{i+1} r_i) I_1(\tau_i r_i) + \frac{\mu_{i+1} \tau_i}{\mu_i \tau_{i+1}} K_1(\tau_{i+1} r_i) I_0(\tau_i r_i) \right] \end{array} \right] \quad (15)$$

Equations (8)–(11) may be written in the following form:

$$A_{i+1} = G^i_{AA} \cdot A_i + G^i_{AC} \cdot C_i \quad (16)$$

$$C_{i+1} = G^i_{CA} \cdot A_i + G^i_{CC} \cdot C_i \quad (17)$$

$$B_{i+1} = G^i_{BB} \cdot B_i + G^i_{BD} \cdot D_i \quad (18)$$

$$D_{i+1} = G^i_{DB} \cdot B_i + G^i_{DD} \cdot D_i. \quad (19)$$

It was noted earlier that we require C_1 and D_1 to be identically zero. Then using (16)–(19) with $i = 1$ results in the following:

$$A_2 = G^1_{AA} \cdot A_1 \quad (20)$$

$$C_2 = G^1_{CA} \cdot A_1 \quad (21)$$

$$B_2 = G^1_{BB} \cdot B_1 \quad (22)$$

$$D_2 = G^1_{DB} \cdot B_1. \quad (23)$$

Using (16)–(19) a second time, with $i = 2$, and (20)–(23) results in the following:

$$A_3 = \left[G^2_{AA} \cdot G^1_{AA} + G^2_{AC} \cdot G^1_{CA} \right] A_1 \quad (24)$$

$$C_3 = \left[G^2_{CA} \cdot G^1_{AA} + G^2_{CC} \cdot G^1_{CA} \right] A_1 \quad (25)$$

$$B_3 = \left[G^2_{BB} \cdot G^1_{BB} + G^2_{BD} \cdot G^1_{DB} \right] B_1 \quad (26)$$

$$D_3 = \left[G^2_{DB} \cdot G^1_{BB} + G^2_{DD} \cdot G^1_{DB} \right] B_1. \quad (27)$$

Continuing this upward cascaded recursion, it is possible to define four γ coefficients as follows:

$$A_M = \gamma_{AA} \cdot A_1 \quad (28)$$

$$C_M = \gamma_{CA} \cdot A_1 \quad (29)$$

$$B_M = \gamma_{BB} \cdot B_1 \quad (30)$$

$$D_M = \gamma_{DB} \cdot B_1 \quad (31)$$

where M is the index of the coaxial dielectric layer just inside the helix.

Equations (12)–(15) may be written in the following form:

$$A_{i-1} = X^i_{AA} \cdot A_i + X^i_{AC} \cdot C_i \quad (32)$$

$$C_{i-1} = X^i_{CA} \cdot A_i + X^i_{CC} \cdot C_i \quad (33)$$

$$B_{i-1} = X^i_{BB} \cdot B_i + X^i_{BD} \cdot D_i \quad (34)$$

$$D_{i-1} = X^i_{DB} \cdot B_i + X^i_{DD} \cdot D_i. \quad (35)$$

It was noted earlier that we require A_N and B_N to be identically zero. Then, using (32)–(35), with $i = N$, results in the following:

$$A_{N-1} = X^N_{AC} \cdot C_N \quad (36)$$

$$C_{N-1} = X^N_{CC} \cdot C_N \quad (37)$$

$$B_{N-1} = X^N_{BD} \cdot D_N \quad (38)$$

$$D_{N-1} = X^N_{DD} \cdot D_N. \quad (39)$$

Using (32)–(35) a second time, with $i = N-1$, and (36)–(39) results in the following:

$$A_{N-2} = \left[X^{N-1}_{AA} \cdot X^N_{AC} + X^{N-1}_{AC} \cdot X^N_{CC} \right] C_N \quad (40)$$

$$C_{N-2} = \left[X^{N-1}_{CA} \cdot X^N_{AC} + X^{N-1}_{CC} \cdot X^N_{CC} \right] C_N \quad (41)$$

$$B_{N-2} = \left[X^{N-1}_{BB} \cdot X^N_{BD} + X^{N-1}_{BD} \cdot X^N_{DD} \right] D_N \quad (42)$$

$$D_{N-2} = \left[X^{N-1}_{DB} \cdot X^N_{BD} + X^{N-1}_{DD} \cdot X^N_{DD} \right] D_N. \quad (43)$$

Continuing this downward cascaded recursion, it is possible to define four ξ coefficients as follows:

$$A_{M+1} = \xi_{AC} \cdot C_N \quad (44)$$

$$C_{M+1} = \xi_{CC} \cdot C_N \quad (45)$$

$$B_{M+1} = \xi_{BD} \cdot D_N \quad (46)$$

$$D_{M+1} = \xi_{DD} \cdot D_N. \quad (47)$$

At the sheath boundary, E_z and E_θ must be continuous. Also, the electric field intensity parallel to the winding (E_{11}) must vanish and the magnetic field intensity parallel to the winding (H_{11}) must be continuous. The fifth condition is that the step in the magnetic field intensity perpendicular to the winding ($H_\perp$) at the sheath boundary must be equal to the sheet current density of

the helix, which is set equal to unity for normalization. Equations (28)–(31) and (44)–(47) may be used with the five equations at the sheath boundary so that the only coefficients remaining are A_1, B_1, C_N, and D_N. The system is overdetermined in respect to the latter four coefficients, so that an error term results.

It is possible to define the following algorithm for solution.

1) Assume a trial value of β.
2) Determine the τ_i by (7).
3) Use cascaded upward recursion to determine the four γ.
4) Use cascaded downward recursion to determine the four ξ.
5) Use the γ and ξ values in the five equations at the helix boundary to solve for A_1, B_1, C_N, and D_N.
6) The system is overdetermined, so an error results. If the error is above tolerance, a correction is made in β and return to Step 2.
7) When the error is sufficiently small, then upward and downward recursion are used to determine the remaining coefficients.

The algorithm has the advantage that no approximation other than the sheath helix model is required. The number of operations necessary to solve the system is linear in N and is dominated by evaluation of the G and X terms. Procedures used for numerical implementation of the algorithm are described in the next section.

III. Numerical Implementation

An efficient iterative scheme must be used to find the complex value of β such that a complex error term is minimized. Müller's method was first proposed as an efficient iterative procedure for finding real and complex roots of a polynomial equation [11]. It has been used successfully with a variety of more general equations, but there has been no proof of convergence in the large [12]. In the present work, an existing algorithm [13] for Müller's method has been used. The Forsythe procedure [12] of deflation is incorporated in the algorithm to allow locating multiple complex roots which correspond to different modes of the electromagnetic fields. It was necessary to modify the procedure for selecting step size in order to obtain a universal routine that has properly converged in all tests made thus far.

IV. Examples

The helical coil has been considered for use in hyperthermia for the treatment of cancer [3]. For a wide range of design parameters, a helical coil in free space will produce an electric field that is essentially parallel with the coil axis, and relatively uniform throughout the cross section of the coil [14], [15]. An incident field with these properties would be expected to produce relatively uniform deposition in a cylinder of lossy dielectric contained within the coil. Experiments with cylindrical fat–muscle phantom models of the human arm and thigh have demonstrated that it is possible to obtain deep, relatively uniform, heating of the muscle-equivalent region [3]. No analysis of this problem has been presented to date.

An inhomogeneous bone/muscle/fat/skin model of the human upper arm was used with the helical coil for numerical testing. Values for the dielectric properties of the tissues were in agreement with those reported by others [16], [17]. The helix had a pitch angle of 3° and a radius of 5.0 cm. The model included layers of teflon 3 and 2 mm in thickness, located just inside and outside the helix, respectively, to support the winding and protect the patient from possible arcing. Dimensions of the complete 8-layer model are given in Table I.

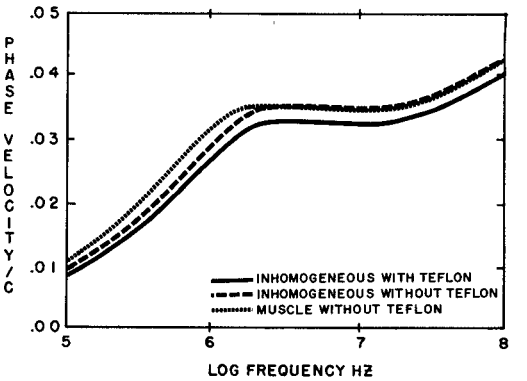

Fig. 1. Phase velocity as a function of frequency for a sheath helix having a lossy dielectric cylinder on its axis.

TABLE I
Inhomogeneous Model for Hyperthermia

Layer	Outer Radius, cm.
Bone	1.2
Muscle	3.4
Fat	3.9
Skin	4.0
Air	4.7
Teflon	5.2
Air	---

The procedures described in this paper were used in the analysis of 1) the model as described in Table I, 2) the model with the teflon layers deleted, and 3) the model with the teflon layers deleted, as well as the cylinder being replaced with homogeneous muscle. No evidence of numerical instability or failures in convergence were found in these tests. Typically, the values of β were found to converge to four-place accuracy in 12 iterations, and six-place accuracy in 15 iterations. Additional (fictitous) layers were added by partitioning various layers into two or more parts having the same dielectric properties, but this caused no significant change in the results. Two or more roots occur at frequencies somewhat over 100 MHz, and they appear to correspond to modes having differing radial dependence.

Fig. 1 shows the phase velocity (normalized relative to the velocity of light in vacuum) as a function of frequency for the basic model and its two variants. The increase of phase velocity with frequency is opposite to that observed for a sheath helix in free space [1] and is attributed to the decrease in permittivity of tissue with increasing frequency. The teflon (dielectric constant of 2.1) causes a decrease in phase velocity at high frequencies, but little change at low frequencies where a larger fraction of the energy is contained within the cylinder. The homogeneous muscle cylinder is similar to the inhomogeneous model at high frequencies where the fields have reduced penetration into the model.

Fig. 2 shows the axial depth as a function of frequency for the basic model and its two variants. Axial depth is defined as the distance measured parallel to the helix axis for which all fields in a traveling wave are reduced in amplitude by a factor of $1/e$. The slight decrease of axial depth caused by the teflon would also be seen with a decrease in helix radius. The axial depth is noticeably greater for the homogeneous muscle cylinder than for the inhomogeneous model.

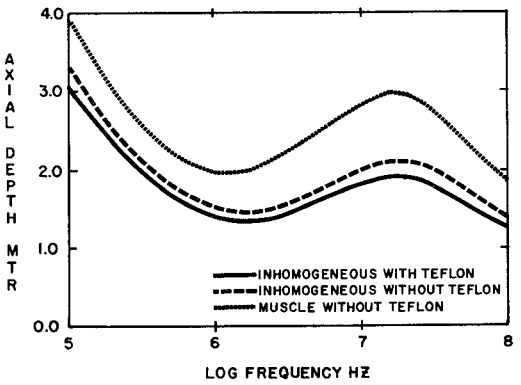

Fig 2 Axial depth as a function of frequency for a sheath helix having a lossy dielectric cylinder on its axis.

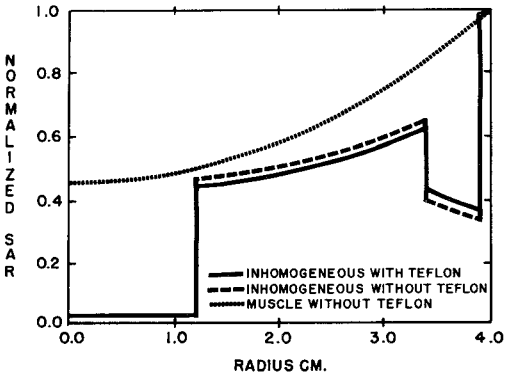

Fig. 3. Normalized SAR as a function of radius in a lossy dielectric cylinder within a sheath helix at 27.12 MHz.

Fig. 3 shows the specific absorption rate (SAR), normalized to the maximum which occurs at the skin surface, as a function of radius for a frequency of 27.12 MHz. The large decrease in energy deposition within the bone and fat layers is largely due to the decreased conductivity of those dielectrics. The fractional change in normalized SAR is more pronounced at the muscle–bone interface than at the muscle–fat or fat–skin interfaces. This is attributed to the fact that the radial component of the electric field is not negligible at the larger radii, so boundary conditions require the magnitude of the electric field to be somewhat greater in the fat layer than in the nearby regions of muscle or skin. The slight increase of deposition in the fat layer and decrease of deposition in the skin layer caused by the teflon would also be seen with a decrease in helix radius, which is consistent with the effect of teflon on axial depth.

The deep, relatively uniform, deposition of energy illustrated in Fig. 3 is in qualitative agreement with experimental results obtained using models with a thermographic camera [3] and confirms that the helical coil shows promise for use as an applicator in hyperthermia.

V. Conclusion

The numerical method described in this paper has been found to be useful for evaluation of the fields of a sheath helix in a coaxially layered lossy dielectric medium. The examples presented pertain to clinical applications and support experimental results suggesting suitability of the helical coil as an applicator in hyperthermia.

Acknowledgment

The author is greatful to Dr. R. S. Chadwick of NIH and Dr. F. W. J. Olver of NBS for valuable suggestions regarding the computation of Bessel functions having complex arguments. The assistance of R. O. Creecy and Dr. R. L. Levin with the computer facilities at NIH is also appreciated.

References

[1] J. R. Pierce, *Traveling-Wave Tubes*. New York: Van Nostrand, 1950.
[2] E. M. El-Sayed and T. K. Abdel-Hamid, "Use of sheath helix slow-wave structure as an applicator in microwave heating systems," *J. Microwave Power*, vol. 16, pp. 283–288, Dec. 1981.
[3] P. S. Ruggera and G. Kantor, "Development of a family of optimized RF helical coil applicator which produce traversely uniform axially distributed heating in cylindrical-muscle phantoms," to be published in *IEEE Trans. Biomed. Eng.*
[4] S. Sensiper, "Electromagnetic wave propagation on helical conductors," Research Laboratory of Electronics, MIT, Tech. Rep. no. 194, May 1951.
[5] P. W. Barber, O. P. Gandhi, M. J. Hagmann, and I. Chatterjee, "Electromagnetic absorption in multilayered model of man," *IEEE Trans. Biomed. Eng.*, vol. BME-26, pp. 400–405, July 1979.
[6] D T. Swift-Hook, "Dispersion curves for a helix in a glass tube," *Proc. IEEE*, vol. 105, pp. 747–755, Dec. 1958.
[7] L. N. Loshakov and E B. Ol'derogge, "Propagation of slow electromagnetic waves along a helix with dielectric supports," *Radio Eng. Electron. Phys.*, vol. 13, pp. 45–51, 1968.
[8] S. Paik, "Design formulas for helix dispersion shaping," *IEEE Trans. Electron Devices*, vol. ED-16, pp. 1010–1014, Dec. 1969.
[9] B. N. Basu, "Equivalent circuit analysis of a dielectric-supported helix in a metal shell," *Int. J. Electron.*, vol. 47, pp. 311–314, Sept. 1979.
[10] G. N. Watson, *A Treatise on the Theory of Bessel Functions*. Cambridge: Cambridge University Press, 2nd ed., 1966.
[11] D. E. Muller, "A method for solving algebraic equations using an automatic computer," *Math. Tables Other Aids Comp.*, vol. 10, pp. 208–215, Oct. 1956.
[12] W. L. Frank, "Finding zeros of arbitrary functions," *J. Ass. Comput. Mach.*, vol. 5, pp. 154–160, Apr. 1958.
[13] S. D. Conte and C. deBoor, *Elementary Numerical Analysis*. New York: McGraw-Hill, 2nd ed., 1972.
[14] F. S. Chute and F. E. Vermeulen, "A visual demonstration of the electric field of a coil carrying a time-varying current," *IEEE Trans. Education*, vol. E-24, pp. 278–283, Nov. 1981.
[15] M. J. Hagmann, "The electromagnetic field of a sheath helix," submitted to *IEEE Trans. Education*.
[16] C. C. Johnson and A. W. Guy, "Nonionizing electromagnetic wave effects in biological materials and systems," *Proc. IEEE*, vol. 60, pp. 692–718, June 1972.
[17] C. H. Durney *et al.*, *Radiofrequency Radiation Dosimetry Handbook*, 2nd ed., University of Utah, Salt Lake City, SAM-TR-78-22, 1978.

Impedance Calculation of Three Narrow Resonant Strips on the Transverse Plane of a Rectangular Waveguide

KAI CHANG, MEMBER, IEEE

***Abstract*—A theoretical analysis has been developed to calculate the impedance of two inductive strips and one capacitive strip located on the transverse plane of a rectangular waveguide. The current ratios among the strips were determined by a variational method and then used for impedance calculations. The results can be applied to the impedance calculations of a single capacitive strip, two inductive strips, or three inductive strips as special cases.**

Manuscript received April 26, 1983; revised August 3, 1983.
The author is with TRW Electronics and Defense, One Space Park, Redondo Beach, CA 90278.

0018-9480/84/0100-0126$01.00 ©1984 IEEE